PHYSICAL REVIEW B VOLUME 52, NUMBER 16 15 OCTOBER 1995-II

Electronic structure of stoichiometric and Ar^+-bombarded ZrO_2 determined by resonant photoemission

C. Morant
Instituto Universitario "Nicolás Cabrera" and Departamento de Física Aplicada C-XII, Universidad Autónoma de Madrid, Cantoblanco, E-28049 Madrid, Spain

A. Fernández and A. R. González-Elipe
Instituto Ciencia de Materiales de Sevilla, Consejo Superior de Investigaciones Científicas, Universidad de Sevilla, Departamento de Química Inorgánica, P.O. Box 1115, E-41071 Sevilla, Spain

L. Soriano
Instituto Universitario "Nicolas Cabrera" and Departamento de Física Aplicada C-XII, Universidad Autónoma de Madrid, Cantoblanco, E-28049 Madrid, Spain

A. Stampfl and A. M. Bradshaw
Fritz-Haber-Institut der Max-Planck-Gesellschaft, Faradayweg 4-6, 14195 Berlin, Germany

J. M. Sanz*
Instituto Universitario "Nicolás Cabrera" and Departamento de Física Aplicada C-XII, Universidad Autónoma de Madrid, Cantoblanco, E-28049 Madrid, Spain

(Received 2 May 1995; revised manuscript received 10 July 1995)

The electronic properties of thermally grown ZrO_2 thin films before and after Ar^+ bombardment have been studied with resonant photoemission spectroscopy using synchrotron radiation. For stoichiometric ZrO_2 thin films the experimental valence-band spectra are in good agreement with the calculated density of states for bulk ZrO_2. For both stoichiometric and Ar^+-bombarded ZrO_2 thin films, resonant photoemission from the valence band was observed when the photon energy was swept through the Zr $4p \rightarrow 4d$ transition energy. The resonant profile was found to exhibit a maximum at $h\nu = 39$ eV, followed by a second well-resolved broad maximum around 50 eV. The feature at 39 eV is consistent with resonant enhancement of the Zr 4*d* states and has been used to identify those regions of the valence band with an important Zr 4*d* admixture. The results are in good agreement with the calculated Zr 4*d* partial density of states. The intensity increase observed at $h\nu \sim 45-50$ eV is found to be associated with the nonbonding region of the valence band, although a proper interpretation is needed. In addition, it was found that Ar^+ bombardment induces electronic states in the band-gap region and changes in the O 2*p* valence band. Three distinct emission bands were identified in the band gap as a function of the Ar^+ dose. They are associated with the formation of oxygen vacancies and mixed oxidation states due to preferential sputtering of the oxygen atoms. Resonant photoemission of these Ar^+-bombarded films demonstrates both the cationic character of the band-gap states and the increase of the cationic contribution to the O 2*p* valence band.

I. INTRODUCTION

The main purpose of this paper is to investigate the electronic structure of thermally grown ZrO_2 thin films as well as the effects induced by Ar^+ bombardment using resonant photoemission spectroscopy (RPES). The electronic band structure of ZrO_2, a refractory transition-metal oxide (TMO), is of great interest from both the technological and fundamental points of view. Its wide use as a high-performance ceramic for nuclear and high-temperature applications, as well as in gas sensing, electro-optical, thin-film, and catalysis applications makes band structure information very important for understanding its physical and chemical properties. Past investigations seem to have been oriented mainly towards practical aspects,[1,2] rather than towards these more fundamental aspects.[3–16] Only a few experiments have probed the electronic structure of ZrO_2,[9–16] and their interpretation has relied on a limited number of band structure calculations.[3–8] Moreover, the electronic structure of defects on transition-metal oxides has also become a subject of extensive study.[17–25] Low-energy ion bombardment is often used to create defects in TMO's, but, because of the difficulty of characterization, its effect on electronic properties has not yet been sufficiently studied. Many spectroscopic studies have shown that oxygen vacancies cause localized energy levels in the band gap. In most cases it has proven difficult, however, to relate the observed electronic states to specific defects, even though this has been attempted recently in some theoretical approaches.[18–21,23] To our knowledge only Sobolev *et al.*,[23] using a self-consistent scattered-wave method,

have tried to study the influence of oxygen vacancies on the electronic structure of ZrO_2. The changes in composition and electronic structure induced in ZrO_2 by 3 keV Ar^+ bombardment have been studied by core and valence-band x-ray photoelectron spectroscopy (XPS) as reported in a recent paper.[26] The results showed that the electronic structure was fairly sensitive to Ar^+ sputtering, a treatment that produces emission features in the band gap and other changes in the O $2p$ region of the valence band (VB), which in turn were ascribed to the formation of oxygen vacancies and suboxides (i.e., reduction). However, the relatively low photoemission cross section of the VB prevented any definitive conclusions from being drawn as to the electronic structure of the stoichiometric and Ar^+-bombarded solid and of the Ar^+-modified surface.

The phenomenon of RPES in transition metals and their compounds has been the subject of many recent investigations.[27–42] A large resonance in the d photoionization cross section is known to occur at photon energies close to the threshold for a $p \rightarrow d$ transition. The resonance process is usually explained as being due to the interference between the direct photoemission process and autoionization of a highly localized excited state created by photoabsorption. Similar effects are found for the valence bands of TMO's even when those have a formal d^0 configuration: It is assumed that the resonance is due to hybridization between the O $2p$ and cation d orbitals. In fact, RPES is used extensively as a method to isolate the d-state contribution and to understand the VB structure of transition-metal compounds and other complex hybridized systems.[27–42] For a detailed discussion the reader is referred to the review by Davis[27] and the book by Henrich and Cox.[25] Studies of the resonant phenomenon itself are also interesting since the details of the resonance in some compounds are not fully understood. For example, extra resonances not directly related to the metal d states have been recently observed in TiO_2 (Ref. 37) and MoS_2,[36] but a satisfactory explanation has not yet been put forward.

In this paper we describe a PES and RPES study of ZrO_2 thin films before and after Ar^+ bombardment aimed at obtaining a better understanding of its valence-band structure and of the changes induced by Ar^+ bombardment. In Sec. II we describe some experimental details and the sample preparation. In Sec. III A we present a comparison of the experimental data with the calculated density of states (DOS) to obtain a reliable picture of the valence-band structure. The RPES study of the ZrO_2 valence band is presented in Sec. III B. A preliminary account of some of these results appeared elsewhere.[14] Section III C is dedicated to the effects induced by Ar^+ bombardment. In Sec. III D we present and discuss the RPES data from a highly reduced surface (i.e., ZrO_x) obtained by Ar^+ bombardment of the original surface. A summary and the conclusions are presented in Sec. IV.

II. EXPERIMENTAL DETAILS

A polycrystalline Zr foil of 99.98% purity from Goodfellow Metals has been used throughout this work. The foil was subjected to the usual cleaning procedures by rinsing in acetone, ethanol, and distilled water before it was introduced into the UHV chamber. The surface was then cleaned by Ar^+ sputtering and annealed under the conditions previously described[43] in order to avoid segregation of impurities which hinder the oxidation. Thermally grown ZrO_2 thin films were obtained by heating the foil at ~ 450 K for longer than 30 min in an oxygen atmosphere ($P_{O_2} \sim 10^{-5}$ Torr). In some cases, after long periods of subsequent exposure to the residual gas some OH adsorption was observed, but could be easily removed by heating at 373 K for short periods.

In order to induce surface defects and changes in stoichiometry the sample was bombarded with Ar^+ ions using an ion gun operated at 0.5 and 2 keV and current densities of $\sim 1\ \mu A\ cm^{-2}$.

The photoemission experiments were performed on the TGM3 monochromator at the Berlin synchrotron radiation source (BESSY) using photon energies between 30 and 70 eV. At these energies the escape depth of the photoelectrons is expected to be less than 10 Å. The angle of incidence of the p-polarized light was 45° with respect to the sample normal. The spectra were recorded at normal emission with an ADES-400 electron energy analyzer. The overall resolution (monochromator + spectrometer) was typically 600 meV. Overview spectra were measured in the constant-retarding-ratio mode, whereas the valence-band spectra in the $0 \leq E_B \leq 14$ eV binding-energy range were taken in the constant-analysis-energy mode with a pass energy of 20 eV. For a more detailed description of the monochromator the reader is referred to the BESSY user's handbook.[44]

All the valence-band spectra presented in this paper have been normalized to the photon flux as measured at a gold mirror at the entrance of the spectrometer chamber. In most cases a background has been subtracted from the spectra using standard methods.[45,46]

III. RESULTS AND DISCUSSION

A. Electronic structure of ZrO_2

Figure 1 shows an overview spectrum of thermally grown ZrO_2 recorded at $h\nu = 50$ eV. The spectrum shows the Zr $4p$ doublet at 30.6 eV, the broad O $2s$ peak at 21.7 eV, and the valence band peaked at 5.3 eV with a clearly distinguishable shoulder at higher energies. The binding energy is referred to the Fermi level of metallic zirconium.

Figure 2 shows the 0–14 eV binding-energy (E_B) range measured with $h\nu = 35$ eV. For comparison we have included the total density of states, as well as the partial oxygen and zirconium densities of states, calculated by Soriano *et al.*[8] for cubic zirconia using the LSW method. The calculated DOS was obtained in terms of the Zr and O $2p$ partial DOS's weighted according to their respective cross sections.[48] For a more detailed description of this procedure see Ref. 8. The overall shape of the experimental curve is well explained by the calculated bulk DOS. The valence band exhibits two distinct structures at ~ 9 and ~ 6 eV binding energy, which according to the

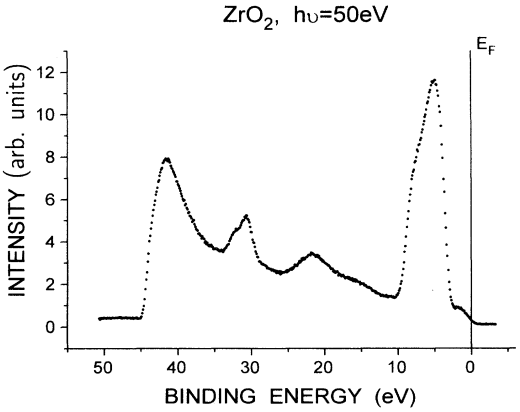

FIG. 1. Photoemission spectrum measured at $h\nu=50$ eV from stoichiometric ZrO_2.

band structure calculation correspond to the bonding O $2p\sigma$ and nonbonding O $2p\pi$ orbitals, respectively, and contain an important zirconium contribution. The Zr contribution is more significant in the higher-binding-energy region, where the bonding O $2p$ orbitals are expected to have a larger admixture of Zr orbitals, and illustrates the importance of the covalent interaction (estimated[8] to be about 24%) in the bonding of ZrO_2. The width of the valence band is estimated to be ~4.8 eV from the energy separation of the points of maximum slope on each side of the band. The valence-band maximum (VBM) is located at ~3.8 eV below the Fermi level as determined by extrapolation of the tangent on the low-binding-energy side of the O $2p$ band. This value is in good agreement with that determined by other electron spectroscopies[11,26] and optical gaps reported in the literature.[15,47]

Apart from the almost classic calculation of Morinaga, Adachi, and Tsukuda[3] based on a discrete variational (DV) $X\alpha$ cluster method, various other attempts have been made to study the electronic structure of ZrO_2. Using the linear-muffin-tin-orbitals (LMTO) method Medvedeva *et al.*[5] have determined the energy band structures of ZrO_2 and other TMO's in order to investigate trends in the band gap and cohesive energy. The band structure of cubic and tetragonal zirconia have been calculated by Jansen[6] using density-functional theory. The structural and electronic properties of cubic and tetragonal zirconia were also explored by Orlando *et al.*[7] using a periodic *ab initio* Hartree-Fock method. Zandiehnadem, Murray, and Ching[4] performed calculations for the three stable phases of ZrO_2 (i.e., monoclinic, cubic, and tetragonal) using the orthogonalized linear combination of atomic orbitals (OLCAO) method, and concluded that the bonding is very similar for the three crystal structures with only minor differences in the width of the band and the band gap. In addition to the general good agreement a result common to all these calculations is the existence of an important covalent bonding contribution, which has been confirmed experimentally with O $1s$ x-ray absorption spectroscopy[12] (XAS) and resonant photoemission.[14] A detailed discussion of these calculations and their comparison with other approaches[8] as well as with experimental photoemission (PES) and bremsstrahlung isochromat (BIS) spectra can be found in Refs. 8 and 13.

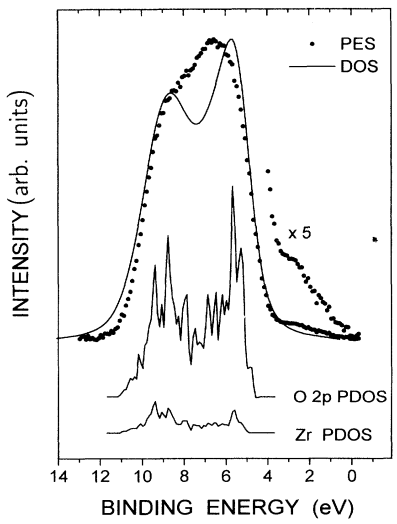

FIG. 2. Calculated bulk DOS (solid line) (see text and Ref. 8 for details) and experimental valence-band photoemission spectrum (points) at $h\nu=35$ eV for stoichiometric ZrO_2. Lower curves: Calculated Zr and O partial densities of states (Ref. 8).

We note that the photoemission intensity of the PES spectra reported here does not fall to zero within the band gap even for the freshly prepared surface. Weak emission in the band gap extends from the top of the valence band up to the Fermi level, showing a maximum at $E_B \approx 2.5$ eV. An expanded view of their contribution is shown in Fig. 2. Usually, such bands are ascribed to trapped electrons in oxygen vacancies and other surface defects[18–26] caused by the preparation method used (i.e., heating at low oxygen pressures). However, by means of a self-consistent scattered-wave method, Sobolev *et al.*[23] have predicted that oxygen vacancies in perfect ZrO_2 crystals are expected to cause trapped electrons in local states within the gap at binding energies between 1.5 and 2 eV, in good agreement with the band observed in this study. A previous XPS study[26] has quantified this effect giving an electron surface density of 6×10^{14} cm^{-2} which is equivalent to a monolayer of oxygen vacancies. It will be shown below that the intensity of this feature can be substantially increased by ion bombardment.

B. Resonant photoemission in ZrO_2

The process of resonant photoemission has been extensively used as a method for isolating the cationic contribution to the valence band of transition-metal compounds. The energy distribution curves (EDC's) from the valence band of ZrO_2 were thus measured at photon energies between 30 and 70 eV as shown in Fig. 3. They indicate that the relative intensities of the two features observed in the valence band are very sensitive to the photon energy due to a resonance process associated with the Zr $4p$ threshold. Although the resonance manifests itself

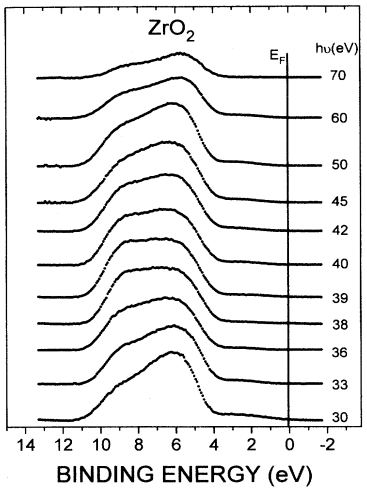

FIG. 3. Valence-band photoemission spectra of ZrO_2 as a function of the photon energy.

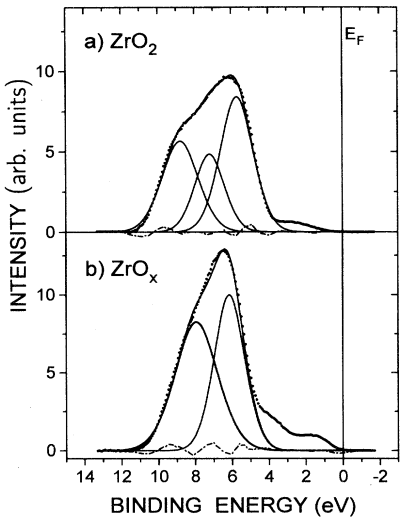

FIG. 4. Analysis of the valence-band photoemission spectrum at $h\nu=50$ eV using three and two Gaussians for ZrO_2 (a) and ZrO_x (b), respectively.

over the whole valence band at photon energies between 36 and 50 eV, the O $2p$ bonding region on the high-binding-energy side of the valence band is enhanced at photon energies around 39 eV. In the case of the spectrum taken at $h\nu=30$ eV the unusually high intensity of the gap states is due to the contribution of the Zr $4p$ core levels excited with second-order light.

In order to study separately the behavior of the bonding and nonbonding contributions to the valence band, we followed a procedure previously used by Zhang, Jeng, and Heinrich[37] in their study of resonance effects in TiO_2. According to these authors the valence-band spectra can be analyzed in terms of three Gaussians, labeled "bonding," "nonbonding," and "overlapping," the widths and energies of which are summarized in Table I for the whole series of spectra. A typical fit is shown in Fig. 4(a) for the VB spectrum measured at $h\nu=50$ eV. Obviously the high- and the low-binding-energy components involve predominantly the bonding and nonbonding orbitals, respectively, whereas the component labeled "overlapping" helps to get a better fit to the valence band.

A more quantitative insight into the resonance effects can be gained by integrating the areas associated with the different components of the valence band and thus generating spectra equivalent to the usual constant-initial-state (CIS) curves. The photon energy dependence of the total intensity of the valence band has thus been depicted in Fig. 5 together with that of the intensity of the bonding, nonbonding, and overlapping components and of the emission band in the gap. The profiles are rather complex and quite unlike the ideal Fano-like curves. In the case of the total valence-band intensity (curve *a*) the profile is characterized by a rise at 36 eV with a maximum at $h\nu=39$ eV, and by a second broad maximum at energies between 45 and 50 eV. The intensity of the bonding component (curve *b*) reaches the main maximum

TABLE I. Best-fit parameters binding energy (E_b) and full width at half maximum (FWHM) for the line shape of the valence band at different photon energies. Three and two Gaussians were used for ZrO_2 and ZrO_x, respectively. The mean, standard deviation (SD), and median value are given for each parameter.

	E_b (eV)			FWHM (eV)		
	Mean	SD	Median	Mean	SD	Median
			ZrO_2			
Bonding	8.74	0.06	8.75	2.32	0.05	2.31
Nonbonding	5.67	0.07	5.68	2.09	0.03	2.10
Overlap	7.14	0.07	7.15	1.89	0.01	1.89
			ZrO_x			
Bonding	8.63	0.09	8.65	2.53	0.07	2.57
Nonbonding	6.51	0.20	6.60	2.57	0.04	2.57

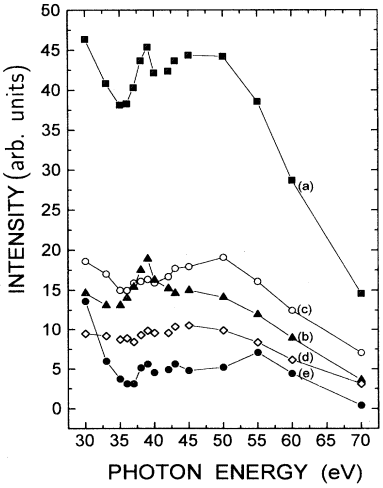

FIG. 5. Photon energy dependence of the integrated intensity of the total valence-band emission (■) (curve *a*) and of the band-gap emission (●) (curve *e*) as well as of the bonding (▲) (curve *b*), nonbonding (○) (curve *c*), and overlapping (◇) (curve *d*) components.

at approximately 39 eV followed by a broad plateau which extends up to 50 eV. On the other hand, the resonance profile of the nonbonding component (curve *c*) consists of a small bump at 39 eV and a gradual rise up to ~50 eV to fall off at higher energies, so that in this case the maximum enhancement of the intensity is produced at photon energies around 45–50 eV. The overlapping component (curve *d*) shows no clear evidence of resonant behavior, but shows rather constant intensity up to 50 eV photon energy. The profile corresponding to the states in the band gap (curve *e*) suggests a weak resonance at 39 eV, but because of the low intensity and possible errors in the background subtraction procedure an unambiguous characterization is difficult. The lack of a systematic picture in the observation of the two resonances (i.e., at 39 and 50 eV) may be linked to the fact that none of the peaks used in the fitting procedure actually correspond to pure bonding or pure nonbonding orbitals.

In order to follow the changes observed in the valence-band shape in a meaningful way, it is useful to compute the 39/36 eV difference spectrum by subtracting the EDC measured at 36 eV (off resonance) from that measured at 39 eV (on resonance). The result is labeled *b* in Fig. 6. The curve labeled *a* corresponds to an XPS valence-band spectrum (i.e., $h\nu=1253.6$ eV) from Ref. 26. For comparison we have included several curves labeled from *c* to *f* which represent the Zr and O PDOS's obtained by different methods. Curves *c* and *f* are the calculated Zr and O 2*p* partial density of states,[8] respectively (see Fig. 2) scaled by the relative photoemission cross sections at $h\nu=1253.6$ eV.[48] Since the Zr 5*s* and Zr 5*p* contributions are negligible, we will use curve *c* to represent the Zr 4*d* density of states. Curves *d* and *e* are intended to represent the O 2*p* density of states. Curve *d* is the valence band of ZrO_2 measured at $h\nu=70$ eV (see Fig. 3), which is expected to reflect the O 2*p* PDOS since the ratio of the O 2*p* and Zr 4*d* photoemission cross sections is >30 at that photon energy.[48] Curve *e* is the result of the subtraction of the Zr contribution as represented by spectrum *b* from the experimental XPS valence band (i.e., curve *a*) (see details below).

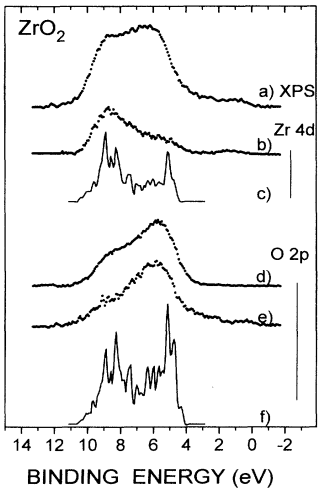

FIG. 6. Curve *a*: XPS spectrum of the valence band from stoichiometric ZrO_2. Curve *b*: Zr 4*d* contribution to the valence band as derived from the resonance at $h\nu=39$ eV. Curve *c*: Calculated Zr partial density of states (from Ref. 8). Curves *d*–*f*: O 2p contribution to the valence band as determined from (curve *d*) photoemission at $h\nu=70$ eV, (curve *e*) the XPS spectrum (*a*) after subtraction of (*b*), and (curve *f*) electronic structure calculations (Ref. 8).

Resonant photoemission of the Zr 4*d* states in ZrO_2 is expected to occur when the photon energy is tuned over the Zr $4p\rightarrow 4d$ transition energy at ~31 eV. The $4p\rightarrow 4d$ transition creates an excited state $[\mathrm{Zr}\ 4p^5 4d^1]^*$ which remains highly localized on the cation site. The excited state can then relax in a direct recombination process which involves the Zr 4*d* states participating in the valence band; i.e., $[\mathrm{Zr}\ 4p^5 4d^1 \mathrm{VB}^n]^* \rightarrow \mathrm{Zr}\ 4p^6 4d^0 \mathrm{VB}^{n-1} + e^-$, which is the same final state as in conventional photoemission. In this manner there is a possible interference between both processes, giving rise to the resonant enhancement of those parts of the spectrum with an important cationic character. In the present study Fig. 6 clearly demonstrates that this is the case for the resonance observed at $h\nu=39$ eV. The good agreement existing between the 39/36 eV difference spectrum, curve *b*, and the calculated Zr 4*d* PDOS,[8] curve *c*, clearly confirms that the phenomenon can be used to identify the Zr-derived states in the valence band. Furthermore, the difference spectrum *b* provides experimental evidence that the partial covalent character of the Zr-O bond is larger in the bonding region than in the nonbonding part of the valence band. Therefore, the bonding contribution should resonate more strongly than the nonbonding one in good agreement with the experimental observation (see Fig. 5). The resonance at $h\nu=39$ eV is then consistent with the resonant photoemission of the Zr 4*d* states and with the assumption of a pure intra-atomic relaxation of the excited state.

It is important to mention here that the resonant photoemission of the *d* states at 39 eV occurs at an 8.4 eV higher energy than the Zr 4*p* binding energy ($E_B=30.6$ eV) as measured by photoemission (see Fig. 1). Similar delays between the threshold (Zr 4*p* binding energy) and the resonance energies have also been observed in metallic Zr (~10 eV),[38,39] as well as in the zirconium nitrides ZrN (~10 eV),[28] and Zr_3N_4 (~11.5 eV), [42] and seem to be a common observation in the lighter transition metals and their compounds.[27] In general, the binding energy of the $[4p^5 4d^{n+1}]^*$ excited state measured from resonant photoemission profiles agrees well with the results of other measurements such as optical absorption or electron-energy-loss spectroscopy (EELS). For ZrO_2, the Zr 4*p* core losses have been shown to exhibit a maximum intensity around 42 eV,[11,49] in reasonable agreement with the energy measured by resonant photoemission.

Figure 6 also allows the comparison between the spectrum assigned to the Zr 4*d* states and the valence-band spectrum obtained by XPS. Interestingly, it is observed that the XPS spectrum is more intense around the top of the valence band (i.e., the nonbonding region). Clearly this is due to the O 2*p*-derived states, because the cationic contributions from Zr 5*s* and Zr 5*p* states are negligible.[8] The O 2*p* states cannot be neglected: although their cross

section at XPS energies is four times lower than that of the Zr 4*d* orbitals,[48] the much larger O 2*p* partial DOS compensates. We have attempted to extract the O 2*p* contribution from the experimental XPS valence band by subtracting the Zr 4*d* contribution determined by resonant photoemission. The result is labeled as *e* in Fig. 6 and shows good agreement with the calculated partial O 2*p* density of states[8] depicted in the same figure as *f*. This agreement is not surprising because the difference was obtained by subtracting a properly scaled difference spectrum, for which the scaling factor was determined by a previous fitting of the experimental XPS valence band in terms of the calculated partial densities of states[8] and the respective cross sections as tabulated by Yeh and Lindau,[48] so that the relative O 2*p*/Zr 4*d* contributions to the valence band were determined according to theoretical calculations.[8]

At present we do not have a satisfactory explanation for the broad resonance occurring at an energy near 50 eV. Recently, Heise and co-workers[40,41] performed a RPES and photoelectron diffraction (XPD) study of the TiO_2(110) surface to determine the Ti 3*d* and O 2*p* valence-band partial densities of states. The RPES results show different displacements of the resonance maxima for different features of the VB, which the authors suggest are associated with different symmetry-resolved initial and final states, although the details of the assignment remain unclear. Assuming a purely intra-atomic direct recombination mechanism, the resonance could be associated with transitions of the Zr $4p \rightarrow$Zr 5*sp* type, where a 4*p* electron is excited into the empty 5*sp* band allowing a resonance with the cationic Zr 5*s* states involved in the valence band of ZrO_2. Obviously, the Zr 5*p* states should not play any role since transitions $4p \rightarrow 5p$ are dipole forbidden. In fact, this mechanism was previously used to explain extra resonances in RPES experiments on TiO_2 (Ref. 37) and MoS_2.[36] The profile of the resonance indicates that in that case the $[\text{Zr } 4p^5 5s^1]^*$ excited state lies 9 eV above the $[\text{Zr } 4p^5 d^1]^*$ state, in good agreement with previous XAS experiment[12] which locate the Zr 5*sp* band ~9 eV above the empty *d* band. However, the calculated Zr 5*s* PDOS does not appear to be intense enough to give rise to the observed enhancement. Unfortunately, the EELS spectra of ZrO_2 do not show any distinguishable feature which could be associated with the resonance at 45 eV; thus either the corresponding excited state is not available with EELS or the excitation cross section is very low.

C. Ar^+ bombardment effects

Figure 7 shows valence-band spectra in the 0–14 eV binding-energy range, taken at $h\nu = 39$ eV (i.e., on resonance), for the initial ZrO_2 surface (lowest curve) and after various degrees of Ar^+ bombardment. In addition, the band-gap region ($4 \text{ eV} \leq E_B \leq 0$) after subtraction of the main O 2*p* valence band is displayed on an expanded scale on the right-hand side of Fig. 7. The figure clearly shows that the electronic structure of ZrO_2 is sensitive to bombardment with Ar^+ ions of 2 keV and that the spectroscopic changes introduced by low-energy sputtering

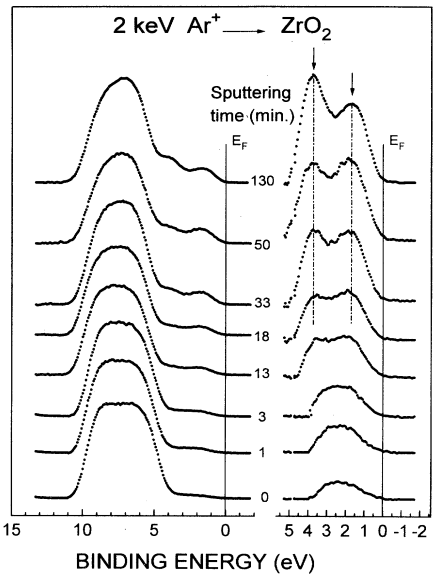

FIG. 7. Photoemission spectra ($h\nu = 39$ eV) of the valence band of ZrO_2 (left) and band-gap emission on an expanded scale (right) as a function of the sputtering time with 2 keV Ar^+ ions.

begin to appear immediately upon bombardment.

The spectra obtained from a fresh ZrO_2 surface as well as after the first three minutes of sputtering exhibit a broad structure of constant shape in the band gap, the intensity of which increases with sputtering time, and whose shape remains unchanged. Its emission maximum is found at $E_B \approx 2.5$ eV and its origin was explained in Sec. III A in terms of oxygen vacancies. At higher Ar^+ doses the structure is observed to develop two additional features around 1.7 and 3.7 eV which also grow upon further Ar^+ bombardment.

In order to follow the different features separately the emission in the band gap was first analyzed by accounting for the broad emission at 2.5 eV. Difference spectra were generated by removing the maximum possible contribution of the original structure (i.e., 0 min) from the spectra at different sputtering times, so that the other two features could be clearly distinguished. These difference spectra are displayed in the inset of Fig. 8 labeled with the scaling factor *F* which was used for each spectrum.

Above 3 min sputtering time (i.e., $\sim 1 \times 10^{16}$ ions cm^{-2}) two peaks at 3.8 and 1.2 eV can be clearly distinguished, and their growth can be followed as the sputtering process proceeds. The integrated intensities of the respective features have been depicted in Fig. 8 as a function of the sputtering time, together with the total intensity of the emission band in the gap. The intensity of the whole emission band induced by Ar^+ ions of 0.5 keV has also been included for comparison. The figure shows that the intensities of the different features and of the whole emission band increase progressively until a stationary state is reached for sputtering times above 60 min (i.e., 2.2×10^{17} ions cm^{-2}).

What is the origin of the three different gap emissions which can be produced by Ar^+ bombardment? The first type is the broad emission at 2.5 eV binding energy,

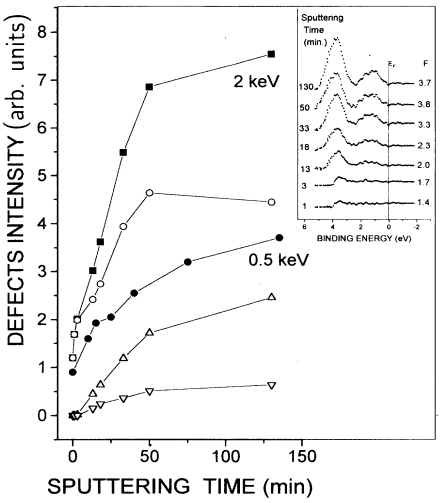

FIG. 8. Intensity of the band-gap emission as a function of the sputtering time with 2 keV (■) and 0.5 keV (●) Ar^+ ions. For 2 keV Ar^+ ions the intensities of three different contributions at 1.2 eV (▽), 2.5 eV (○), and 3.8 eV (△) have been included. Inset: band-gap emission after subtraction of the spectrum at 0 min scaled with a factor F.

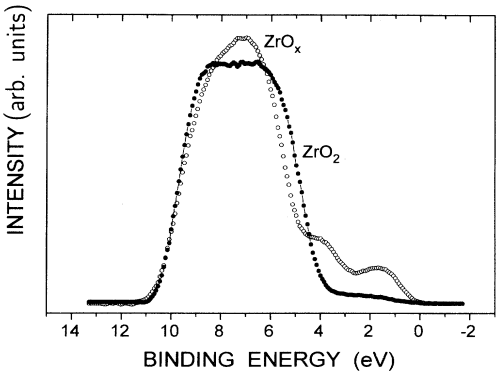

FIG. 9. Valence-band photoemission spectra from both stoichiometric ZrO_2 and reduced ZrO_x measured at $h\nu=39$ eV.

which forms after any degree of reduction of the surface and is present even on a fresh ZrO_2 surface. It has been assigned to electrons trapped on oxygen vacancies that populate the 4d orbitals of adjacent Zr atoms. The measured energy of this band is in good agreement with the calculations by Sobolev *et al.*[23] using a self-consistent scattered-wave method.[23] Furthermore, Munnix and Schmeits[19] have also shown that an emission band around 1.3 eV observed in TiO_2 could be accounted for by subsurface oxygen vacancies. In fact, it seems to be a general finding in TMO's that oxygen vacancies induce electronic states in the band gap.[18–25]

At higher Ar^+ dose the increase in the concentration of oxygen vacancies produces more complex defect structures and even significant changes of stoichiometry.[26] This is probably the origin of the two sharp features observed only after heavy reduction of the surface (i.e., high-defect-density surfaces). The high-binding-energy feature at 3.8 eV we assign to bulk Zr-O vacancy complexes associated with the formation of lower oxidation states (i.e., Zr^{3+}, Zr^{2+}). Furthermore, the band can be related to an optical absorption at 3.31 eV observed in cubic zirconia and attributed to sixfold-coordinated Zr^{3+} by Azzoni and Paleari using electron paramagnetic resonance.[50] In contrast, the weakest band observed at 1.2 eV requires still heavier reduction to be unambiguously distinguished. It is tentatively ascribed to the formation of small clusters of Zr^+ and even Zr^0 in the limiting species of the sputtering process when Ar^+ bombardment produces much higher defect densities, and more electrons populate the Zr 4d orbitals. In fact, the formation of mixed oxidation states (i.e., Zr^{3+}, Zr^{2+}, Zr^+, and Zr^0) has been demonstrated by XPS.[26] The cationic character of all these band-gap states is confirmed by the resonant photoemission spectra shown below.

Although the most significant effect of the Ar^+ bombardment is the growth of the emission features in the gap, the O 2p valence band is also observed to undergo changes. Figure 9 compares the valence-band photoemission spectra for the stoichiometric and severely reduced surfaces. In general, we observed a decrease in the valence-band width and an increase in its intensity due to the presence of additional reduced cations, which increase the d contribution. The valence band maximum moves 0.45 eV away from the Fermi level (i.e, band bending) as a consequence of the reduction of the surface. In fact, it is well established that electrons trapped in oxygen vacancies occupy localized empty orbitals of the cations, pushing up the Fermi level and bending the whole electronic structure to higher binding energies.

Figure 10 shows photoemission spectra of ZrO_x after its exposure to increasing amounts of O_2 at temperatures between 298 and 473 K (as labeled). The figure shows rather clearly that an oxygen exposure of 100 L at 298 K causes a significant decrease in the intensity of the gap states. On the contrary, practically no change is observed in the shape of the O 2p band. Only after exposures above 300 L at 423 K does the valence-band spectrum recover the shape of that for ZrO_2. Thus, although generation of states in the band gap and modification of the valence-band shape occur simultaneously during Ar^+ bombardment, the second effect remains even after removal of the oxygen vacancies by O_2 adsorption at low temperatures. This fact suggests that the shape could be related to the amorphization and loss of the three-dimensional order of ZrO_2 by Ar^+ bombardment. Furthermore, according to these results the modified structure characterized by a higher covalency (see below) is preserved until the structure is annealed above 423 K.

In order to observe any possible influence from the ion energy we performed a similar detailed study of the effects induced by 0.5 keV Ar^+ ions. The effects are qualitatively very similar to those discussed above for 2 keV Ar^+ ions, but not so intense. After a similar sputtering time we observed that the steady state reached at 0.5 keV consists of an altered layer with considerably fewer defects than that obtained by sputtering with 2 keV Ar^+ ions (Fig. 8). In the following resonant photoemission experiments on the reduced surface using 0.5 keV ions are described.

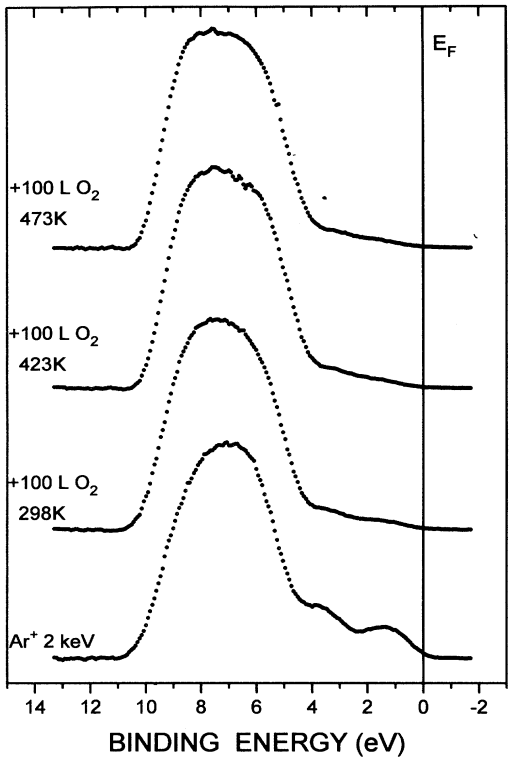

FIG. 10. Photoemission spectra ($h\nu=39$ eV) of the valence band of ZrO_x (2 keV Ar^+ ions) after oxygen exposure at increasing temperatures.

D. Resonant photoemission of ZrO_x

Figure 11 shows an overview photoemission spectrum taken after bombardment with 0.5 keV Ar^+ ions for 135 min (i.e., steady state). Compared with the spectrum of ZrO_2 in Fig. 1 the effects of Ar^+ bombardment are clearly observable in all the bands including the Zr 4*p*, the O 2*s*, the O 2*p*, and the emission band in the gap. The Zr 4*p* peak is broadened, suggesting that Zr species having valence states lower than 4+ are now present. The Zr 4*p*/O 2*s* intensity ratio increases upon ion bombardment, confirming the preferential loss of oxygen. An estimation of the surface composition in terms of the Zr 4*p* and O 2*s* intensities gives an average stoichiometry $ZrO_{1.1}$ which is in good agreement with the average composition ($\sim$ZrO) of the altered layer caused by 3 keV Ar^+ ions, as determined by XPS.[26] In Fig. 12 we show the valence-band photoemission spectra of ZrO_x in the 0–15 eV binding-energy region, measured at photon energies in the range $30 \leq h\nu \leq 60$ eV. On the right-hand side of the figure, the band-gap emission has been depicted on an expanded scale. Again, the intensity and shape of the gap states measured at $h\nu=30$ eV are strongly affected by the contribution of the Zr 4*p* core levels excited with second-order light and will not be considered in the quantitative analysis.

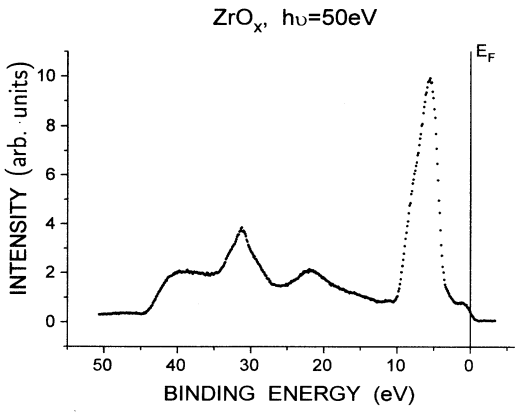

FIG. 11. Photoemission spectrum measured at $h\nu=50$ eV from ZrO_2 after bombardment with 0.5 keV Ar^+ ions (135 min).

Effects associated with the resonant process are clearly observable and have been quantitatively analyzed in a similar manner to that for stoichiometric ZrO_2 in Sec. III B. Figure 13 shows the dependence of the photon energy with respect to the intensity of the valence band and the emission in the band gap. Again we show the behavior of the respective intensities of two Gaussians labeled as "bonding" and "nonbonding." In this case, however, the valence-band spectra could be analyzed in terms of only two of such curves, the widths and energy positions of which are summarized in Table I. A typical fit is shown in Fig. 4(b). The Gaussian labeled as nonbonding is assigned to the lowest-binding-energy component, whereas the bonding one has been assigned to the highest-binding-energy component.

The resonance profiles of Fig. 13 show a behavior similar to those measured for stoichiometric ZrO_2. In particular, all the profiles are characterized by two maxima around 40 eV and 45–50 eV. Whereas the intensity of the bonding component reaches its main maximum at 40 eV, we note that the resonance profile of the nonbonding component shows a bump at that energy followed by an

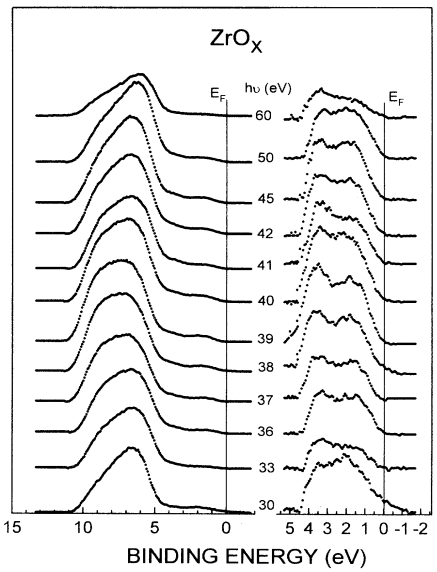

FIG. 12. Photoemission spectra of the valence band (left) and the band-gap emission (right) from ZrO_x (see Fig. 11) as a function of the photon energy.

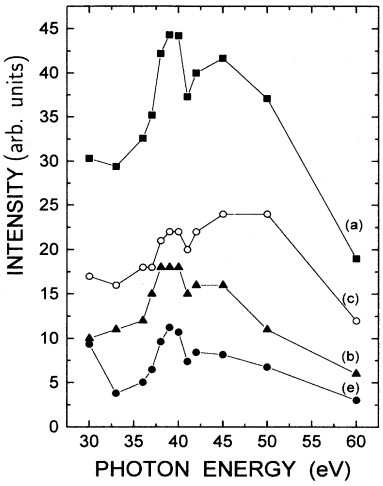

FIG. 13. Photon energy dependence of the integrated intensity of the total valence band (■) (curve *a*) and the band-gap emission (●) (curve *e*) as well as of the bonding (▲) (curve *b*) and nonbonding (○) (curve *c*) components.

absolute maximum at ~50 eV. The resonance at 40 eV is associated with the enhancement of the Zr 4*d* states involved in the valence band, while the origin of the resonance at 45–50 eV is unknown. The resonant behavior of the states in the band gap is more clearly observed in this case due to the increased intensity in this spectral region. The maximum at 40 eV clearly confirms the cationic character of these states. All the profiles show that the resonance at 40 eV has broadened significantly compared with the sharp peak observed for stoichiometric ZrO_2.

As in Sec. III B we calculated difference curves in order to point out those regions of the spectra which are enhanced when the energy of resonance is reached. The resulting curve obtained after subtracting the photoemission spectra measured at 36 eV (off resonance) from that measured at 40 eV (on resonance) is shown in Fig. 14. This figure also includes the XPS valence-band spectrum

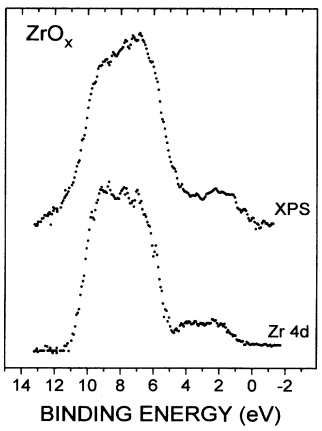

FIG. 14. Zr 4*d* contribution to the valence band as determined from the resonances at $h\nu=40$ eV. For comparison we have included the XPS spectrum of the valence band of ZrO_x from Ref. 26.

of ZrO_2 bombarded with 3 keV Ar^+ ions published in Ref. 26. According to the interpretation given above the 40/36 eV difference spectrum should reflect the Zr 4*d* partial density of states in ZrO_x; unfortunately, there are not band structure calculations for comparison. Comparing with the equivalent spectrum for ZrO_2 (see Fig. 6) indicates a significant increase in the Zr 4*d* contribution, mainly in the low-binding-energy region of the valence band (i.e., the nonbonding region), as a result of the sputtering. The increase in the cationic contribution clearly suggests a significant increase in covalency due to the preferential loss of oxygen atoms and the corresponding reduction of the cation. This effect is also confirmed by comparing the 40/36 eV difference curve, labeled Zr 4*d* in Fig. 14, with the XPS valence band of ZrO_x obtained after bombardment with 3 keV Ar^+ ions.[26] Contrary to the comparison made in Fig. 6 for ZrO_2, we observe in the case of ZrO_x reasonable agreement between the XPS valence-band spectrum and the Zr 4*d* contribution represented by the difference curve 40/36 eV. This indicates that the O 2*p* contribution to the valence band of ZrO_x is quantitatively less important than for ZrO_2. The small differences should be accounted for by the O 2*p* contribution. A comparison between the analysis of the XPS valence band for ZrO_2 (Fig. 6) and ZrO_x (Fig. 14) leads to the conclusion that whereas the O 2*p* component is significantly reduced in intensity the Zr 4*d* contribution increases over the width of the valence band but more strongly in the nonbonding region. Although the cationic component is probably overestimated, the data indicate that the creation of oxygen vacancies and the heavy reduction of the oxide by Ar^+ bombardment causes a significant decrease in the number of ionic Zr-O bonds and a considerable increase in covalency for the modified surface.

IV. SUMMARY AND CONCLUSIONS

The electronic structure of thermally grown ZrO_2 thin films before and after Ar^+ bombardment was studied with resonant photoemission spectroscopy using synchrotron radiation. Good agreement has been found between the valence-band spectra of thermally grown ZrO_2 thin films and the calculated density of states for bulk ZrO_2. For both stoichiometric and Ar^+-bombarded ZrO_2 thin films, resonant photoemission from the valence band was observed when the photon energy was tuned through the Zr $4p \rightarrow 4d$ transition energy. A rather complex dependence of the total valence-band intensity on the photon energy was found. The resonance profile exhibits a maximum at $h\nu=39$ eV followed by a second broad structure at 45–50 eV. The intensity enhancement observed at 39 eV is consistent with the resonant photoemission of Zr 4*d* states involved in the valence band. In fact, the phenomenon has been used to identify those regions of the valence band with an important Zr 4*d* character and also to estimate the degree of Zr 4*d*/O 2*p* hybridization. The second resonance at photon energies between 45 and 50 eV is associated with the nonbonding region of the valence band; however, its origin remains unexplained. In addition, we have studied the changes that occur in

the electronic structure of ZrO_2 when it is reduced by Ar^+ bombardment. The latter treatment induces electronic states in the band-gap region as well as significant changes in the O 2*p* band. Three distinct emission bands induced by the Ar^+ bombardment have been identified. A broad emission band at 2.5 eV binding energy is assigned to oxygen vacancies; it forms after any degree of reduction and exists even on the freshly grown films. The other two emission bands at 1.2 and 3.8 eV are observed after further oxygen loss at Ar^+ doses $>3\times10^{15}$ ions cm^{-2}. They appear to be associated with the formation of more complex defect structures and the presence of several lower oxidation states of zirconium, leading to a severe reduction of the oxide within the modified surface layer. Resonant photoemission of these Ar^+-bombarded films indicates an important increase in the cationic contribution to the valence band (i.e., an increased covalency) as well as the Zr 4*d* character of the band-gap states.

ACKNOWLEDGMENTS

The authors are pleased to acknowledge the financial support of the CICYT and DGICYT of Spain through Contracts No. MAT93/0805, No. MAT94/1039, and No. PB93-0240 and the European Union through Contracts Nos. ERBCHRXCT 930358 and BESSY-CHGE-CT93-0027 under the Human Capital and Mobility Programme.

*Author to whom correspondence should be addressed. Fax: 34-1-3973969; electronic address: jomasanz@ccuam3.sdi.uam.es

[1]*Zirconia '88. Advances in Zirconia Science and Technology,* edited by S. Meriani (Elsevier, New York, 1989), and references therein.
[2]A. H. Heuer, J. Am. Ceram. Soc. **70**, 689 (1987).
[3]M. Morinaga, M. Adachi, and M. Tsukuda, J. Phys. Chem. Solids **44**, 301 (1983).
[4]F. Zandiehnadem, R. A. Murray, and W. Y. Ching, Physica B **150**, 19 (1988).
[5]N. I. Medvedeva, V. P. Zhukov, M. Ya. Khodos, and V. A. Gubanov, Phys. Status Solidi B **160**, 517 (1990).
[6]H. J. F. Jansen, Phys. Rev. B **43**, 7267 (1991).
[7]R. Orlando, C. Pisani, C. Roetti, and E. Stefanovich, Phys. Rev. B **45**, 592 (1992).
[8]L. Soriano, M. Abbate, J. Faber, C. Morant, and J. M. Sanz, Solid State Commun. **93**, 659 (1995).
[9]J. Frandon, B. Brousseau, and F. Pradal, Phys. Status Solidi B **98**, 379 (1980).
[10]P. Camagni, P. Galinetto, G. Samoggia, and N. Zema, Solid State Commun. **83**, 943 (1992).
[11]F. Yubero, J. M. Sanz, E. Elizalde, and L. Galán, Surf. Sci. **237**, 173 (1990); F. Yubero, J. M. Sanz, J. F. Trigo, E. Elizalde, and S. Tougaard, Surf. Interface Anal. **22**, 124 (1994).
[12]L. Soriano, M. Abbate, J. C. Fuggle, M. A. Jiménez, J. M. Sanz, C. Mythen, and H. A. Padmore, Solid State Commun. **87**, 699 (1993).
[13]L. Soriano, M. Abbate, D. Alders, and J. M. Sanz, Solid State Commun. **91**, 551 (1994).
[14]J. M. Sanz, A. R. González-Elipe, A. Fernández, D. Leinen, L. Galán, A. Stampfl, and A. M. Bradshaw, Surf. Sci. **307-309**, 848 (1994).
[15]R. H. French, S. J. Glas, F. S. Ohuchi, Y.-N. Xu, and W. Y. Ching, Phys. Rev. B **49**, 5133 (1994).
[16]P. Camagni, G. Samoggia, L. Sangaletti, F. Parmigiani, and N. Zema, Phys. Rev. B **50**, 4292 (1994).
[17]V. E. Henrich, G. Dresselhaus, and H. F. Zeiger, Phys. Rev. Lett. **36**, 1355 (1976).
[18]S.-il Choi and T. Takeuchi, Phys. Rev. Lett. **50**, 1474 (1983).
[19]S. Munnix and M. Schmeits, Phys. Rev. B **31**, 3369 (1985).
[20]S. Munnix and M. Schmeits, Phys. Rev. B **33**, 4136 (1986).
[21]D. F. Cox, T. B. Fryberger, and S. Semancik, Phys. Rev. B **38**, 2072 (1988).
[22]J. M. Themlin, R. Sporken, J. Darville, R. Caudano, and J. M. Gilles, Phys. Rev. B **42**, 11 914 (1990).
[23]A. B. Sobolev, A. N. Varaksin, O. A. Keda, and A. P. Khaimenov, Phys. Status Solidi B **162**, 165 (1990).
[24]Y. Aiura, F. Iga, Y. Nishihara, H. Ohnuki, and H. Kato, Phys. Rev. B **47**, 6732 (1993).
[25]V. E. Henrich and P. A. Cox, *The Surface Science of Metal Oxides* (Cambridge University Press, Cambridge, England, 1994).
[26]C. Morant, J. M. Sanz, and L. Galán, Phys. Rev. B **45**, 1391 (1992).
[27]L. C. Davis, J. Appl. Phys. **59**, R25 (1986).
[28]R. D. Bringans and H. Höchst, Phys. Rev. B **30**, 5416 (1984).
[29]E. Bertel, R. Stockbauer, and T. E. Madey, Phys. Rev. B **27**, 1939 (1983).
[30]E. Bertel, R. Stockbauer, R. L. Kurtz, T. E. Madey, and D. E. Ramaker, Surf. Sci. **152/153**, 776 (1985).
[31]B. Cord and R. Courths, Surf. Sci. **162**, 34 (1985).
[32]Y. Ueda, H. Negishi, M. Koyano, M. Inoue, K. Soda, H. Sakamoto, and S. Suga, Solid State Commun. **57**, 839 (1986).
[33]K. E. Smith and V. E. Henrich, Solid State Commun. **68**, 29 (1988).
[34]K. E. Smith and V. E. Henrich, Phys. Rev. B **38**, 9571 (1988).
[35]R. Courths, B. Cord, and H. Saalfeld, Solid State Commun. **70**, 1047 (1989).
[36]J. R. Lince, S. V. Didziulis, and J. A. Yarmoff, Phys. Rev. B **43**, 4641 (1991).
[37]Z. Zhang, S.-P. Jeng, and V. E. Henrich, Phys. Rev. B **43**, 12 004 (1991).
[38]C. G. H. Walker, P. K. Hucknall, D. Greig, M. J. Walker, J. Turton, J. A. D. Matthew, and D. Norman, Solid State Commun. **82**, 573 (1992).
[39]C. G. H. Walker, P. K. Hucknall, J. A. D. Matthew, D. Norman, D. Greig, M. J. Walker, and J. Turton, Surf. Sci. **269/270**, 610 (1992).
[40]R. Heise, R. Courths, and S. Witzel, Solid State Commun. **84**, 599 (1992).
[41]R. Heise and R. Courths, Surf. Sci. **287/288**, 658 (1993).
[42]P. Prieto, A. Fernández, L. Soriano, F. Yubero, E. Elizalde, A. R. González-Elipe, and J. M. Sanz, Phys. Rev. B **51**, 17 984 (1995).
[43]C. Morant, J. M. Sanz, L. Galán, L. Soriano, and F. Rueda, Surf. Sci. **218**, 331 (1989).
[44]*Research at Bessy. A User's Handbook,* edited by Ch. Jung (BESSY, Berlin, 1993).
[45]D. A. Shirley, Phys. Rev. B **5**, 4709 (1972).
[46]H. E. Bishop, Surf. Interface Anal. **3**, 272 (1981).
[47]R. S. Sokolova, Sov. J. Appl. Phys. **41**, 454 (1974).
[48]J. J. Yeh and I. Lindau, At. Nucl. Data Tables **32**, 1 (1985).
[49]J. M. Sanz and C. Palacio, Solid State Commun. **64**, 189 (1987).
[50]C. B. Azzoni and A. Paleari, Phys. Rev. B **44**, 6858 (1991).